JACS
JOURNAL OF THE AMERICAN CHEMICAL SOCIETY
Article
pubs.acs.org/JACS

Regioselective Benzyl Radical Addition to an Open-Shell Cluster Metallofullerene. Crystallographic Studies of Cocrystallized $Sc_3C_2@I_h$-C_{80} and Its Singly Bonded Derivative

Hongyun Fang,[†,∇] Hailin Cong,[‡,∇] Mitsuaki Suzuki,[#,§,∥,∇] Lipiao Bao,[†] Bing Yu,[‡] Yunpeng Xie,[†] Naomi Mizorogi,[#] Marilyn M. Olmstead,*[,¶] Alan L. Balch,*[,¶] Shigeru Nagase,[⊥] Takeshi Akasaka,*[,†,#,§,∥] and Xing Lu*[,†]

[†]State Key Laboratory of Materials Processing and Die & Mold Technology, School of Materials Science and Engineering, Huazhong University of Science and Technology (HUST), Wuhan, 430074, China

[‡]Lab for New Fiber Materials and Modern Textile-Growing Base for State Key Laboratory, College of Chemical and Environmental Engineering, Qingdao University, Qingdao 266071, China

[#]Life Science Center of Tsukuba Advanced Research Alliance, University of Tsukuba, Tsukuba, Ibaraki 305-8577, Japan

[§]Foundation for Advancement of International Science, Tsukuba, Ibaraki 305-0821, Japan

[∥]Department of Chemistry, Tokyo Gakugei University, Koganei, Tokyo 184-8501, Japan

[¶]Department of Chemistry, University of California, Davis, California 95616, United States

[⊥]Fukui Institute for Fundamental Chemistry, Kyoto University, Kyoto 606-8103, Japan

Supporting Information

ABSTRACT: The endohedral fullerene once erroneously identified as $Sc_3@C_{82}$ was recently shown to be $Sc_3C_2@I_h$-C_{80}, the first example of an open-shell cluster metallofullerene. We herein report that benzyl bromide (**1**) reacts with $Sc_3C_2@I_h$-C_{80} via a regioselective radical addition that affords only one isomer of the adduct $Sc_3C_2@I_h$-$C_{80}(CH_2C_6H_5)$ (**2**) in high yield. An X-ray crystallographic study of **2** demonstrated that the benzyl moiety is singly bonded to the fullerene cage, which eliminates the paramagnetism of the endohedral in agreement with the ESR results. Interestingly, X-ray results further reveal that the 3-fold disordered Sc_3C_2 cluster adopts two different configurations inside the cage. These configurations represent the so-called "planar" form and the computationally predicted, but not crystallographically characterized, "trifoliate" form. It is noteworthy that this is the first crystallographic observation of the "trifoliate" form for the Sc_3C_2 cluster. In contrast, crystallographic investigation of a $Sc_3C_2@I_h$-C_{80}/Ni(OEP) cocrystal, in which the endohedral persists in an open-shell structure with paramagnetism, indicates that only the former form occurs in pristine $Sc_3C_2@I_h$-C_{80}. These results demonstrate that the cluster configuration in EMFs is highly sensitive to the electronic structure, which is tunable by exohedral modification. In addition, the electrochemical behavior of $Sc_3C_2@I_h$-C_{80} has been markedly changed by the radical addition, but the absorption spectra of the pristine and the derivative are both featureless. These results suggest that the unpaired electron of $Sc_3C_2@I_h$-C_{80} is buried in the Sc_3C_2 cluster and does not affect the electronic configuration of the cage.

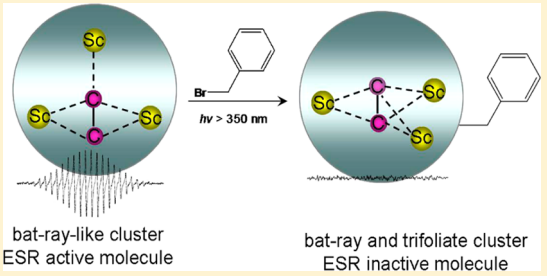

INTRODUCTION

The rich electronic properties and the spherical shape of fullerenes engender them ideal platforms for further derivatization.[1−6] Whereas exohedral attachment of different functional groups onto fullerene surfaces has generated numerous organic materials with applications in such fields as biology and photovoltaics, endohedral metal doping of fullerenes represents another novel strategy that produces a new class of hybrid molecules: endohedral metallofullerenes (EMFs).[2−7] During the last two decades, many EMFs containing a variety of metallic species have been synthesized and characterized.

The chemistry of EMFs has recently become a main concern of researchers because chemical modification is an effective way to create applicable materials.[8,9] The results of several studies have shown that the chemical properties of cage carbons are highly susceptible to the location, motion, and electronic configuration of the encapsulated metallic species.[8] On the other hand, it is also believed that exohedral modification is a practical tool to control the location and configuration of the internal metallic clusters.[10]

Among the chemical transformations that have been applied to functionalize EMFs, radical addition produces stable derivatives that normally bear different properties from the

Received: June 12, 2014
Published: July 7, 2014

 © 2014 American Chemical Society dx.doi.org/10.1021/ja505858y | J. Am. Chem. Soc. 2014, 136, 10534−10540

original EMFs because of the single bond formation.[11] However, an obvious disadvantage of radical addition is the undesired formation of multiple adducts because of the high reactivity of radicals. For instance, both photochemical perfluoroalkylation of La@C_{82}-B[12] and thermal trifluoromethylation of Y@C_{82}[13] afforded mixtures of multi-adducts, respectively. The latter method was also applied to functionalize Sc_3N@C_{80}, and an even number of addends, from 2 to 16, were present in the derivatives.[14] Recently, a highly regioselective radical addition to Sc_3N@C_{80} exclusively afforded a bisadduct with a 1,4-addition pattern.[15]

In contrast, radical additions to some paramagnetic mono-EMFs, either readily soluble or completely insoluble in common organic solvents, gave rise to corresponding derivatives with a singly bonded substituent, such as La@C_{2n}($C_6H_3Cl_2$) ($2n$ = 72, 74, 80, 82).[16−21] These results indicate that the chemical properties of EMFs strongly depend on the electronic structures of the internal metallic species. Nevertheless, it is still unclear whether the electronic and geometric configurations of the endohedral metallic cluster are tunable through exohedral modification on the cage surface.

Sc_3C_2@I_h-C_{80} is a unique cluster EMF that had been erroneously assigned as Sc_3@C_{82}.[22,23] Sc_3C_2@I_h-C_{80} has an open-shell electronic configuration that differs from other cluster EMFs, which are closed-shell molecules. Computational results proposed that an unpaired electron is trapped inside the cluster rather than delocalized on the cage, a situation which is consistent with its EPR-active property.[24,25] Theoretically, an early study indicated that the Sc_3C_2 cluster can adopt either a trifoliate (idealized D_{3h}) structure or a planar (idealized C_{2v}) structure and that these are mutually isoenergetic.[23,24] A second computational report[25] emphasized the dynamical nature of the cluster and the existence of multiple minimum energy structures where the C_2 unit undergoes a flipping motion. A recent crystallographic study indicated that the planar structure is present in the open-cage adamantylidene derivative of Sc_3C_2@I_h-C_{80} which retains the paramagnetism of the parent EMF,[23] but the situation in unfunctionalized Sc_3C_2@I_h-C_{80} remains unknown. Furthermore, it is also of special interest to know the Sc_3C_2 cluster configuration in a closed-shell derivative of Sc_3C_2@I_h-C_{80} that can be obtained by radical addition onto the cage surface.

Herein, we report that benzyl bromide (**1**) reacts with Sc_3C_2@I_h-C_{80} via a regioselective radical addition that affords only one isomer of the adduct Sc_3C_2@I_h-C_{80}($CH_2C_6H_5$) (**2**) in high yield. Single crystal X-ray crystallographic results for the benzyl derivative Sc_3C_2@I_h-C_{80}($CH_2C_6H_5$), **2**, clearly demonstrate that the Sc_3C_2 cluster adopts two different configurations: one that resembles the theoretically predicted trifoliate structure and one that places the C_2 unit angled above the triangle of scandium ions, termed a bat ray structure. In contrast, X-ray crystallographic results from a Sc_3C_2@I_h-C_{80}/Ni(OEP) cocrystal indicate that the cluster configuration in pristine Sc_3C_2@I_h-C_{80} exists in a single, bat ray form, the one with the C_2 unit angled above the triangle of scandium ions. These results suggest that exohedral modification is an effective way to alter the internal cluster structures in EMFs.

EXPERIMENTAL SECTION

High-performance liquid chromatography (HPLC) was conducted on an LC-908 instrument (Japan Analytical Industry Co., Ltd.) using toluene as the mobile phase. Matrix-assisted laser desorption/ionization time-of-flight (MALDI-TOF) mass spectra were measured on a BIFLEX III spectrometer (Bruker, Germany) using 1,1,4,4-tetraphenyl-1,3-butadiene as matrix. Vis-NIR spectra were measured on a LAMBDA 750 UV/vis/NIR spectrophotometer (PerkinElmer, US) in CS_2. Cyclic voltammetry (CV) and differential pulse voltammetry (DPV) were measured in 1,2-dichlorobenzene with 0.1 M (n-Bu)$_4$NPF$_6$ at a Pt working electrode on a CHI610E workstation. The scan rate was 20 mV s^{-1} and the pulse amplitude of DPV was 50 mV.

Black single crystals of Sc_3C_2@I_h-C_{80}($CH_2C_6H_5$) **2** were obtained by layering hexane over a CS_2 solution of **2** at 273 K for 2 weeks. Sc_3C_2@I_h-C_{80}/Ni(OEP) cocrystals were similarly grown from CS_2/benzene. X-ray data were collected at 90 K with a Bruker Apex II diffractometer. The multiscan method was used for absorption corrections. The structures were solved with the use of direct methods and were refined using SHELXL-2014.[26−28]

Geometry optimization calculations of Sc_3C_2@I_h-C_{80}/NiOEP were achieved with hybrid density functional theory at the M06-2X/3-21G level for Sc and for C atoms.[29−31] Calculations were carried out using the GAUSSIAN 09.[32]

Sc_3C_2@I_h-C_{80} was synthesized with a modified arc discharge method and was isolated with multistage HPLC. In a typical reaction, a flask containing 40 mL of a toluene solution of 5 mg Sc_3C_2@ I_h-C_{80} and an excess amount (ca. 50-fold) of benzyl bromide (**1**) was degassed with argon for 10 min. Then the mixture was photoirradiated with a mercury-arc lamp (cutoff <350 nm) at room temperature (Figure 1a).

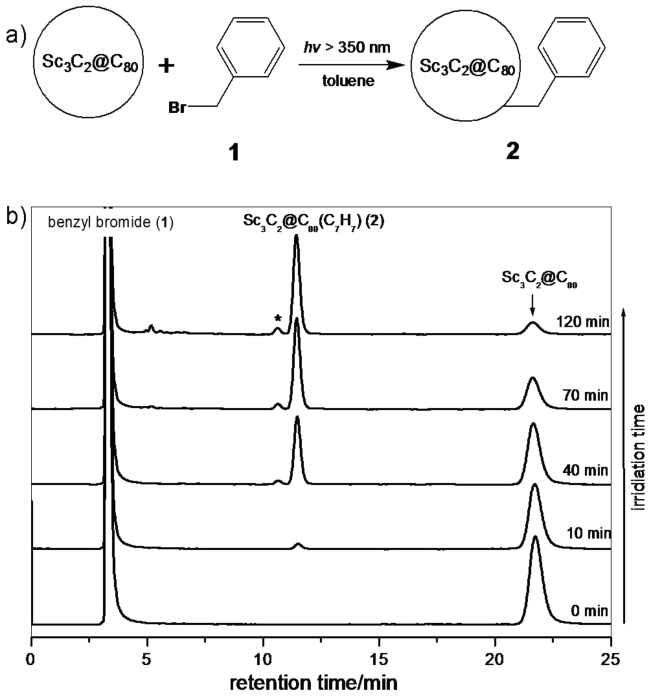

Figure 1. (a) Schematic illustration of the photochemical reaction between Sc_3C_2@C_{80} and **1**. (b) HPLC tracing of the reaction on a PYE column. Conditions: 20 μL injection volume; 1.0 mL/min toluene flow; 330 nm detection wavelength; 298 K. The asterisk denotes an unidentified product.

RESULTS AND DISCUSSION

The reaction progress was monitored with HPLC (Figure 1b). Before irradiation, the two starting materials presented strong peaks at 3.3 min for **1** and 21.6 min for Sc_3C_2@I_h-C_{80}, respectively. After the solution was irradiated for 10 min, a new peak ascribed to monoadduct **2** appeared at 11.4 min. The content of **2** continued to increase, while the concentration of

dx.doi.org/10.1021/ja505858y | J. Am. Chem. Soc. 2014, 136, 10534−10540

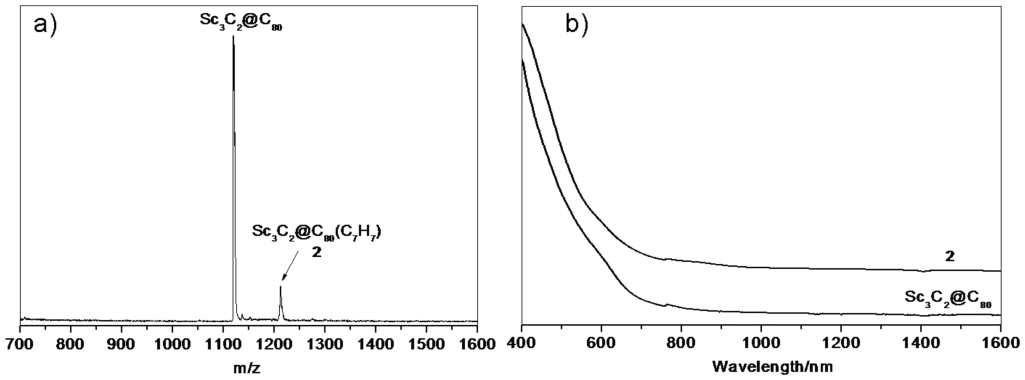

Figure 2. (a) MALDI-TOF spectrum of **2** under a negative linear condition and (b) vis-NIR spectra of $Sc_3C_2@C_{80}$ and **2**.

$Sc_3C_2@C_{80}$ decreased simultaneously upon irradiation. The reaction was terminated when a small amount of bis-adducts was formed. Finally, the product **2** was isolated in a yield higher than 95% based on consumed $Sc_3C_2@C_{80}$ (Figure S1, Supporting Information).

A MALDI-TOF mass spectrometric study firmly confirms the attachment of the benzyl moiety onto the fullerene cage (Figure 2a). The molecular ion peak of $Sc_3C_2@C_{80}(C_7H_7)$ (**2**) is clearly observed at m/z 1210. Observation of a more pronounced peak of bare $Sc_3C_2@C_{80}$ at m/z 1119 implies the single bond character between the benzyl moiety and the fullerene cage. This is consistent with the ESR-silent property of **2** (Figure S2, Supporting Information). Detachment of the substituents from the fullerene cages by laser irradiation has been frequently observed in previous mass spectroscopic studies of EMF-derivatives, especially of those singly bonded adducts.[33]

The electronic structure of **2** resembles that of $Sc_3C_2@I_h$-C_{80}. Both compounds show essentially identical absorption spectra, largely featureless curves in the wavelength range between 400 and 1600 nm (Figure 2b). These spectra are similar to the absorption spectra of other $M_3N@I_h$-C_{80} species and indicate that the unpaired electron is buried inside the cluster in $Sc_3C_2@I_h$-C_{80} and the cage has an electronic configuration of $[C_{80}]^{6-}$.[34] Even though the radical addition has eliminated the unpaired electron, the cage-based electronic structure of $Sc_3C_2@C_{80}$ is not changed much, suggesting that both the pristine EMF and the adduct have the $[C_{80}]^{6-}$ electronic structure.

To accurately determine the addition pattern and the cluster configurations in **2**, a single crystal X-ray diffraction study was performed.[27] The asymmetric unit contains an entire molecule of **2** with 1.5 CS_2 solvent molecules, one disordered at a center of symmetry and the other featuring three disordered positions. The cage shows no disorder, but the Sc_3C_2 cluster is disordered inside the cage. In the C_2 unit, one carbon atom (C1C) is fully ordered and appears in each of the three cluster orientations, whereas three others have occupancies with ratios of 0.63:0.20:0.17 for C2C, C3C, and C4C, respectively. The C−C distances are 1.116(8) Å for C1C−C2C, 1.051(15) Å for C1C−C3C, and 1.044(15) Å for C1C−C4C. These values are indicative of C≡C triple bond character but are shorter than the values calculated for $Sc_3C_2@C_{80}$ (1.27−1.35 Å),[24,25] possibly as an artifact of the C_2 motion and reduced occupancy. As to the three Sc^{3+} ions, the two close to the site of addition are completely occupied, but the one distant from the addend possesses two disordered sites with a ratio of 0.83:0.17.

Figure 3 shows the X-ray structure of **2** with the major metal sites paired with the major C_2-unit orientation. The benzyl

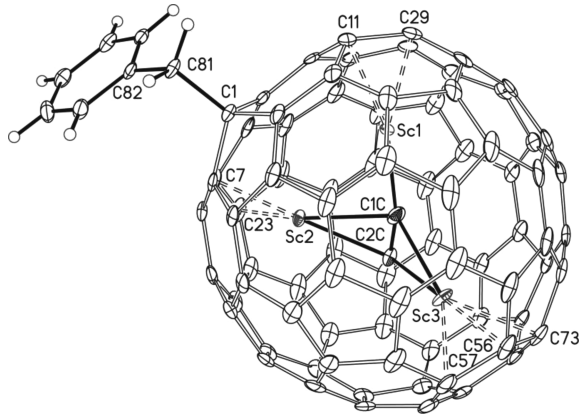

Figure 3. A view of $Sc_3C_2@I_h(7)$-$C_{80}(CH_2C_6H_5)$, **2**, showing the major orientation (63% for C2C and 83% for Sc3) of the cluster. Thermal ellipsoids are drawn at the 25% probability level. The key distances from Sc to cage carbons are indicated on the drawing. These are Sc1−C11, 2.171(4) Å; Sc1−C29, 2.165(4) Å; Sc2−C7, 2.191(3) Å; Sc2−C23, 2.172(4) Å; Sc3−C56, 2.192(4) Å; Sc3−C57, 2.270(4) Å; and Sc3−C73, 2.236(4) Å. The C−C distance from the cage to the addend, C1−C81, is 1.558(5) Å.

group is singly bonded to a carbon atom at a [5,6,6]-juncture of the I_h-C_{80} cage. This site is typically more reactive than a cage carbon at a [6,6,6]-junction as shown in previous reports on $Sc_3N@C_{80}$ derivatives.[13,14] The length of the C−C bond formed between the benzyl moiety and the cage is 1.558(5) Å, which is consistent with single C−C bond character. The two metal atoms Sc1 and Sc2, which are close to the site of addition, approach the nearby [5,6]-bond junctions with Sc−C distances ranging from 2.165(4) to 2.191(3) Å. In contrast, the remaining scandium atom Sc3, which is far from the addend and is a bit disordered, is situated over a [6,6]-junction with longer Sc−C distances from 2.192(4) to 2.236(4) Å. The pyramidalization of the C1 carbon is large, in keeping with its sp^3 character. Also, the cage carbons nearest to the Sc's have pyramidalization angles of ca. 14° compared to ca. 10° for carbons not impacted by close contact to Sc (Figure S4, Supporting Information).

The cluster configurations in **2** were analyzed in further detail, which provides some surprising results. As shown in Figure 4, three forms are present. In each, the Sc_3C_2 unit deviates significantly from the planarity. The major and one of

dx.doi.org/10.1021/ja505858y | J. Am. Chem. Soc. 2014, 136, 10534−10540

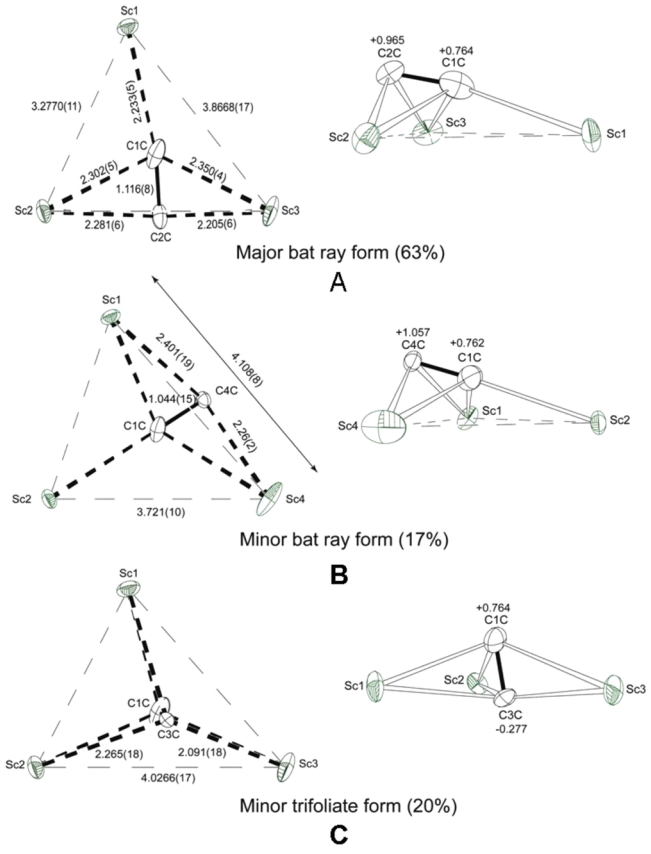

Figure 4. Geometric features of the encaged cluster in the benzyl adduct **2**. The top two views (Parts A and B) show the bat ray form. The bottom view (Part C) is the "trifoliate" cluster. The major bat ray form and the minor trifoliate form use the same set of scandium positions, while the minor bat ray form employs Sc1, Sc2, and Sc4. Carbide atom C1C is used in all three forms, but different carbon atoms are present in each of the three forms. The vertical displacements of these atoms above and below the respective Sc_3 planes are indicated above the carbon atoms. Distances are in Å.

the minor forms we have termed as bat ray structures. In the top drawing of the major bat ray form, the line C2C−C1C−Sc1 defines the direction of the tail of the bat ray, while the triangles C2C−C1C−Sc2 and C2C−C1C−Sc3 define its wings. Some dimensions of the clusters are provided in the figure. In the major bat ray structure, the C1C/C2C line subtends an angle of 10.4° to the Sc_3 plane, while in the minor bat ray form, the corresponding angle is 16.4°. In the bottom view, the trifoliate-like orientation is created by the 81.9° tipping of the C1C−C3C line from the Sc_3 plane. However, the C_2 unit is asymmetrically positioned with regard to the Sc_3 plane. Thus, C1C is 0.764 Å above the plane, while C3C is only −0.277 Å below the plane. This is the first crystallographic observation of the trifoliate form.

The cluster configuration in **2** may differ from the situation in pristine $Sc_3C_2@I_h$-C_{80} because the electronic configuration and the cage structure have been altered by the benzyl radical addition. To examine this issue, we prepared cocrystals of $Sc_3C_2@I_h$-C_{80} with Ni(OEP) (OEP is the dianion of octaethylporphyrin) in which the EMF is not covalently functionalized, and accordingly the situation more resembles that of pristine $Sc_3C_2@I_h$-C_{80}. A high-quality crystal was characterized with X-ray crystallography.[28] The crystal falls into the monoclinic *C*2/*m* space group, in which two halves of the cage and a Ni(OEP) molecule reside on a crystallographic mirror plane.

Figure 5 shows the X-ray structure of $Sc_3C_2@I_h$-C_{80}/Ni(OEP) with the major components encapsulated inside a

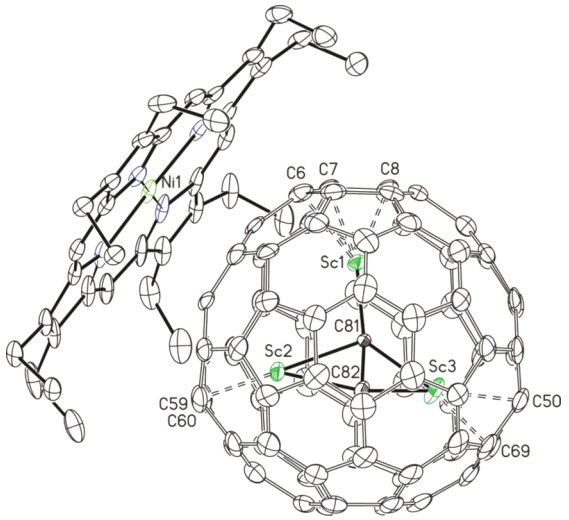

Figure 5. A view of $Sc_3C_2@I_h(7)$-C_{80}·Ni(OEP) showing the major (82%) cluster orientation. Thermal ellipsoids are drawn at the 25% probability level. The key distances from Sc to cage carbon atoms are indicated on the drawing. These distances are Sc1−C6, 2.253(17) Å; Sc1−C7, 2.129(12) Å; Sc1−C8, 2.163(18) Å; Sc2−C59, 2.150(14) Å; Sc2−C60, 2.10(4) Å; Sc3−C50, 2.188(9) Å; and Sc3−C69, 2.095(15) Å.

cage orientation. The nearest cage−Ni distance is 2.707(7) Å, which is consistent with a $\pi-\pi$ interaction. Each of the three scandium atoms approaches an adjacent [5,6]-bond junction, and the Sc−C(cage) distances are comparable to these found in the derivative **2**. Pyramidalization angles are again greater for those carbons closest to encaged Sc atoms (see Figure S4, Supporting Information). The C_2 unit is displaced to one side of the plane of the three scandium ions. The C−C distance is 1.286(14)Å, in agreement with computations. One of the three Sc atoms shows two disordered positions (Sc1:Sc4 = 0.82:0.18), whereas the other two Sc atoms, Sc2 and Sc3, are fully occupied, enabling accurate determination of the cluster configurations.

Inside the cage, the five-atom cluster adopts a configuration with the C_2-line deviating from the Sc_3 plane by 7.2° for the major bat ray form, as shown in Figure 6. For the minor site of the disordered Sc atom (18% occupancy), the angle between the C_2 moiety axis and the Sc_3 plane is a bit larger, 9.1°. Again, the two carbon atoms apart from the Sc_3 plane by 0.417 and 0.629 Å, respectively. These configurations are not coplanar structures but bat ray structures, which are consistent with theoretical results (vide infra).

Parts A and B of Figure 7 shows the structures of the Sc_3C_2 cluster obtained in the computational study of Taubert et al.[25] As the drawings show, the geometries of the two forms of the cluster differ from the idealized planar (pseudo-C_{2v}) and trifoliate (pseudo-D_{3h}) structures, but they do resemble the structures obtained from the crystallographic study. Part C of Figure 7 shows the Sc_3C_2 cluster that results from the computations reported here. Note the similarity of this drawing to the bat ray forms in Figures 4 and 6. Usually, the more common M_2C_2 fragments in endohedral fullerenes adopt a

dx.doi.org/10.1021/ja505858y | J. Am. Chem. Soc. 2014, 136, 10534−10540

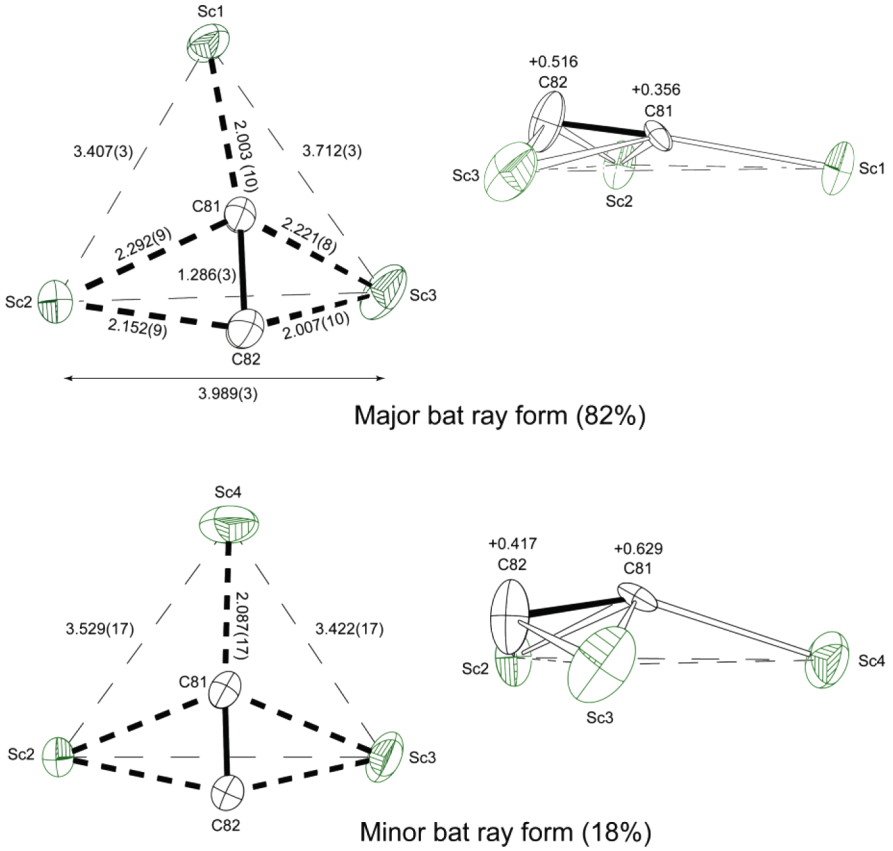

Figure 6. Geometric features of the major and minor bat ray forms of the Sc_3C_2 cluster in $Sc_3C_2@I_h$-C_{80}. The carbide carbon atoms do not reside within the plane of the three scandium ions. The vertical displacements of these atoms above the respective Sc_3 planes are indicated above the carbon atoms. Distances are in Å.

butterfly arrangement with a variable dihedral angle between the two MC_2 planes (the butterfly wings). In this context, the cluster shapes seen in Parts A and B of Figure 4 and in part A of Figure 7 adopt a bat ray configuration. In Part A of Figure 4, the arrangement of bat ray wings involves Sc1, Sc2, C1C, and C2C, and the line from C1C to Sc3 forms the tail. In this arrangement, Sc1 and Sc2 can interact with the two π-bonds of the acetylide, while Sc3 interacts with C1C in a σ-bond fashion to form the tail.

Considering that the trifoliate configuration becomes possible in the singly bonded derivative **2**, it is concluded that exohedral functionalization of EMFs can effectively change the cluster configurations. Previous computational works have demonstrated that the spin-unpaired electron in $Sc_3C_2@I_h$-C_{80} is localized on the internal cluster rather than on the cage.[25] Since the benzyl radical addition eliminates the spin on the cluster, as demonstrated by ESR analysis (Figure S2, Supporting Information), it subsequently affects the cluster configuration as well. It is now reasonable to conclude that the cluster configuration of Sc_3C_2 is strongly dependent on the electronic structure of the endohedral.

From the X-ray results of $Sc_3C_2@I_h$-C_{80}/NiOEP and **2**, we found that the fullerene cage has not been markedly distorted upon radical addition. Except for the carbon at the site of addition, which has been pulled out to retain its sp^3-character, and carbons the nearest to the Sc ions, which bear larger POAV values, the other carbon atoms have similar POAV values to one another (Figure S4, Supporting Information).

The cyclic voltammogram of **2** exhibits two reversible reduction steps and a less reversible oxidation process (Figure 8), while the previous studies showed pristine $Sc_3C_2@C_{80}$ displays three reduction processes and one oxidation process.[23] The first reduction potential of **2** is cathodically shifted by 0.22 V, as compared to that of $Sc_3C_2@C_{80}$, although their oxidation potentials are nearly identical. As a result, the singly bonded derivative **2** has a larger electrochemical bandgap (0.68 V) than pristine $Sc_3C_2@C_{80}$ (0.47 V), suggesting an enhanced stability of the derivative, which should attribute to its closed-shell electronic configuration. Relevant electrochemical results are summarized in Table 1.

■ CONCLUSION

Regioselective addition of benzyl radicals, generated *in situ* by photoirradiation of benzyl bromide (**1**), to a paramagnetic trimetallic carbide metallofullerene, $Sc_3C_2@I_h$-C_{80}, afforded a sole derivative (**2**) with the benzyl moiety singly bonded to a [5,6,6]-juncture cage carbon. X-ray crystallographic results of **2** reveal that the Sc_3C_2 cluster adopts both bat wing and trifoliate structures. This is the first time crystallographic evidence of the trifoliate structure has been found. In contrast, X-ray data of $Sc_3C_2@I_h$-C_{80}/Ni(OEP) cocrystals demonstrate that only the bat wing structure is more favorable in pristine $Sc_3C_2@I_h$-C_{80}, confirming a substantial influence of the exohedral modification on the electronic and geometric configurations of the internal cluster. Our work has not only presented a useful method for the synthesis of stable EMF-derivatives but has also shed new

dx.doi.org/10.1021/ja505858y | J. Am. Chem. Soc. 2014, 136, 10534−10540

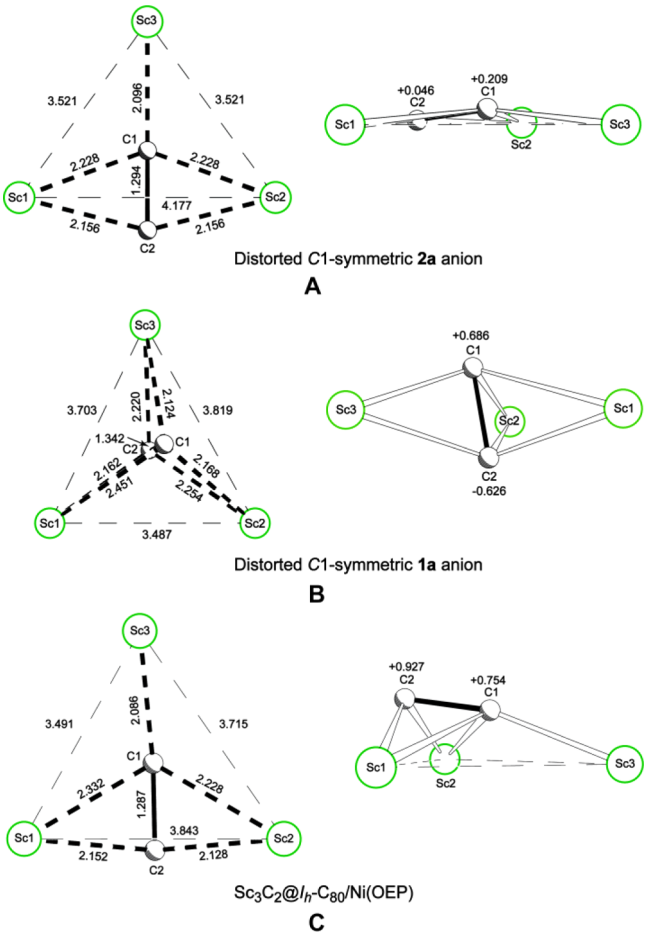

Figure 7. Computed geometric features of the Sc_3C_2 cluster in $Sc_3C_2@I_h$-C_{80}. Parts A and B were drawn from the data in ref 25. Part C shows the results of the computations reported here. The carbide carbon atoms do not reside within the plane of the three scandium ions. The vertical displacements of these atoms above and below the respective Sc_3 planes are indicated above the carbon atoms. Distances are in Å.

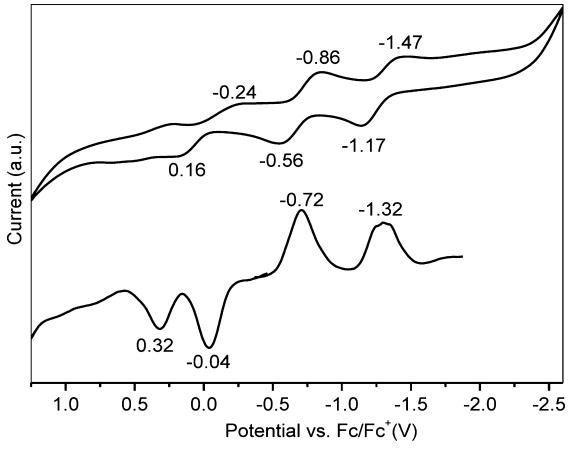

Figure 8. CV and DPV graphs of **2** on a Pt electrode in 1,2-dichlorobenzene containing 0.1 M $(n\text{-Bu})_4NPF_6$ as supporting electrolyte.

light on the cluster configurations inside the confined nanospaces of fullerene cages.

Table 1. Redox Potentials[a] (V vs Fc/Fc^+) of $Sc_3C_2@C_{80}$ and 2

compound	$^{ox}E_2$	$^{ox}E_1$	$^{red}E_1$	$^{red}E_2$	ΔE^c
$Sc_3C_2@C_{80}$[b]	–	−0.03	−0.50	−1.64	0.47
2	+0.32	−0.04	−0.72	−1.32	0.68

[a]DPV values on a Pt-working electrode in 1,2-dichlorobenzene containing 0.1 M $(n\text{-Bu})_4NPF_6$. [b]Ref 23. [c]$\Delta E = {}^{ox}E_1 - {}^{red}E_1$.

■ ASSOCIATED CONTENT

Ⓢ Supporting Information

Chromatographic and ESR spectroscopic results of **2**, X-ray data of $Sc_3C_2@I_h$-C_{80}/Ni(OEP) and **2** in CIF format, the optimized structure of $Sc_3C_2@I_h$-C_{80}/Ni(OEP), and results of the POAV (pyramidalization) analysis of **2** and $Sc_3C_2@I_h$-C_{80}/Ni(OEP). This material is available free of charge via the Internet at http://pubs.acs.org.

■ AUTHOR INFORMATION

Corresponding Authors

lux@hust.edu.cn
mmolmstead@ucdavis.edu
albalch@ucdavis.edu
akasaka@tara.tsukuba.ac.jp

Author Contributions

▽These authors contributed equally.

Notes

The authors declare no competing financial interest.

■ ACKNOWLEDGMENTS

Financial support from The National Thousand Talents Program of China, NSFC (21171061, 21271067), 973 Project of China (2012CB722705), Program for Changjiang Scholars and Innovative Research Team in University (IRT1014), the Fok Ying Tong Education Foundation of China (131045) to X.L., KAKENHI from MEXT Japan (20108001, 202455006, and 24350019), The Strategic Japanese-Spanish Cooperative Program funded by JST and MICINN to T.A. and the NSF Grants CHE-1305125 and CHE-1011760 to A.L.B. and M.M.O. is gratefully acknowledged.

■ REFERENCES

(1) Hirsch, A.; Brettreich, M. *Fullerenes-Chemistry and Reactions*; Wiley-VCH: Weinheim, 2005.
(2) Chaur, M. N.; Melin, F.; Ortiz, A. L.; Echegoyen, L. *Angew. Chem., Int. Ed.* **2009**, *48*, 7514−7538.
(3) Yamada, M.; Akasaka, T.; Nagase, S. *Acc. Chem. Res.* **2010**, *43*, 92−102.
(4) Rodriguez-Fortea, A.; Balch, A. L.; Poblet, J. M. *Chem. Soc. Rev.* **2011**, *40*, 3551−3563.
(5) Lu, X.; Feng, L.; Akasaka, T.; Nagase, S. *Chem. Soc. Rev.* **2012**, *41*, 7723−7760.
(6) Lu, X.; Akasaka, T.; Nagase, S. *Acc. Chem. Res.* **2013**, *47*, 1627−1635.
(7) Popov, A.; Yang, S.; Dunsch, L. *Chem. Rev.* **2013**, *113*, 5989−6113.
(8) Lu, X.; Akasaka, T.; Nagase, S. *Chem. Commun.* **2011**, *47*, 5942−5957.
(9) Maeda, H.; Tsuchiya, T.; Lu, X.; Takano, Y.; Akasaka, T.; Nagase, S. *Nanoscale* **2011**, *3*, 2421−2429.
(10) Shustova, N. B.; Chen, Y. S.; Mackey, M. A.; Coumbe, C. E.; Phillips, J. P.; Stevenson, S.; Popov, A. A.; Boltalina, O. V.; Strauss, S. H. *J. Am. Chem. Soc.* **2009**, *131*, 17630−17637.

(11) Tzirakis, M. D.; Orfanopoulos, M. *Chem. Rev.* **2013**, *113*, 5262−5321.
(12) Tagmatarchis, N.; Taninaka, A.; Shinohara, H. *Chem. Phys. Lett.* **2002**, *355*, 226−232.
(13) Kareev, I. E.; Lebedkin, S. F.; Bubnov, V. P.; Yagubskii, E. B.; Ioffe, I. N.; Khavrel, P. A.; Kuvychko, I. V.; Strauss, S. H.; Boltalina, O. V. *Angew. Chem., Int. Ed.* **2005**, *44*, 1846−1849.
(14) Shustova, N. B.; Peryshkov, D. V.; Kuvychko, I. V.; Chen, Y. S.; Mackey, M. A.; Coumbe, C.; Heaps, D.; Confait, B. S.; Heine, T.; Phillips, J. D.; Stevenson, S.; Dunsch, L.; Popov, A.; Strauss, S. H.; Boltalina, O. V. *J. Am. Chem. Soc.* **2011**, *133*, 2672−2690.
(15) Shu, C.; Slebodnick, C.; Xu, L.; Champion, H.; Fuhrer, T.; Cai, T.; Reid, J.; Fu, W. J.; Harich, K.; Dorn, H. C.; Gibson, H. W. *J. Am. Chem. Soc.* **2008**, *130*, 17755−17760.
(16) Nikawa, H.; Kikuchi, T.; Wakahara, T.; Nakahodo, T.; Tsuchiya, T.; Rahman, G. M. A.; Akasaka, T.; Maeda, Y.; Yoza, K.; Horn, E.; Yamamoto, K.; Mizorogi, N.; Nagase, S. *J. Am. Chem. Soc.* **2005**, *127*, 9684−9685.
(17) Wakahara, T.; Nikawa, H.; Kikuchi, T.; Nakahodo, T.; Rahman, G. M. A.; Tsuchiya, T.; Maeda, Y.; Akasaka, T.; Yoza, K.; Horn, E.; Yamamoto, K.; Mizorogi, N.; Slanina, Z.; Nagase, S. *J. Am. Chem. Soc.* **2006**, *128*, 14228−14229.
(18) Nikawa, H.; Yamada, T.; Cao, B. P.; Mizorogi, N.; Slanina, Z.; Tsuchiya, T.; Akasaka, T.; Yoza, K.; Nagase, S. *J. Am. Chem. Soc.* **2009**, *131*, 10950−10954.
(19) Akasaka, T.; Lu, X.; Kuga, H.; Nikawa, H.; Mizorogi, N.; Slanina, Z.; Tsuchiya, T.; Yoza, K.; Nagase, S. *Angew. Chem., Int. Ed.* **2010**, *49*, 9715−9719.
(20) Lu, X.; Nikawa, H.; Kikuchi, K.; Mizorogi, N.; Slanina, Z.; Tsuchiya, T.; Akasaka, T.; Nagase, S. *Angew. Chem., Int. Ed.* **2011**, *50*, 6356−6359.
(21) Lu, X.; Nikawa, H.; Tsuchiya, T.; Akasaka, T.; Toki, M.; Sawa, H.; Mizorogi, N.; Nagase, S. *Angew. Chem., Int. Ed.* **2010**, *49*, 594−597.
(22) Takata, M.; Nishibori, M.; Sakata, M.; Yamamoto, E.; Inakuma, M.; Shinohara, H. *Phys. Rev. Lett.* **1999**, *83*, 2214−2217.
(23) Iiduka, Y.; Wakahara, T.; Nakahodo, T.; Tsuchiya, T.; Sakuraba, A.; Maeda, Y.; Akasaka, T.; Yoza, K.; Horn, E.; Kato, T.; Liu, M. T. H.; Mizorogi, N.; Kobayashi, K.; Nagase, S. *J. Am. Chem. Soc.* **2005**, *127*, 12500−12501.
(24) Tan, K.; Lu, X. *J. Phys. Chem. A* **2006**, *110*, 1171−1176.
(25) Taubert, S.; Straka, M.; Pennanen, T. O.; Sundholma, D.; Vaara, J. *Phys. Chem. Chem. Phys.* **2008**, *10*, 7158−7168.
(26) Sheldrick, G. M. *Acta Crystallogr.* **2008**, *A64*, 112−122.
(27) Crystal data for **2**, $Sc_3C_2@I_h(7)$-C_{80}benzyl·1.5CS_2: $C_{90.5}H_7S_3Sc_3$, M_w = 1325.02, monoclinic, space group $P2_1/c$, a = 11.053(2) Å, b = 18.656(4) Å, c = 22.247(4) Å, β = 96.86(3)°, V = 4554.6(15) Å^3, Z = 4, T = 90(2) K, ρ_{calcd} = 1.932 Mg m^{-3}, μ(MoKα) = 0.643 mm^{-1}, 55165 reflections measured, 12056 unique (R_{int} = 0.048) used in all calculations. The final $wR2$ was 0.2535 (all data) and $R1$ (10712 with $I > 2\sigma(I)$) = 0.0866.
(28) Crystal data for $Sc_3C_2@I_h(7)$-C_{80}Ni(OEP)·1.5(benzene)·CS_2: $C_{128}H_{53}N_4NiS_2Sc_3$, M_w = 1904.45, monoclinic, space group $C2/m$, a = 26.788(3) Å, b = 16.9531(19) Å, c = 17.6337(17) Å, β = 106.517(6)°, V = 7677.7(14) Å^3, Z = 4, T = 90(2) K, ρ_{calcd} = 1.648 Mg m^{-3}, μ(MoKα) = 0.620 mm^{-1}, 17689 reflections measured, 7007 unique (R_{int} = 0.039) used in all calculations. The final $wR2$ was 0.2501 (all data) and $R1$ (4842 $I > 2\sigma(I)$) = 0.0813.
(29) Becke, A. D. *Phys. Rev. A* **1988**, *38*, 3098−3100.
(30) Becke, A. D. J. *Chem. Phys.* **1993**, *98*, 5648−5652.
(31) Lee, C.; Yang, W.; Parr, R. G. *Phys. Rev. B* **1988**, *37*, 785−789.
(32) Frisch, M. J.; Trucks, G. W.; Schlegel, H. B.; Scuseria, G. E.; Robb, M. A.; Cheeseman, J. R.; Scalmani, G.; Barone, V.; Mennucci, B.; Petersson, G. A.; Nakatsuji, H.; Caricato, M.; Li, X.; Hratchian, H. P.; Izmaylov, A. F.; Bloino, J.; Zheng, G.; Sonnenberg, J. L.; Hada, M.; Ehara, M.; Toyota, K.; Fukuda, R.; Hasegawa, J.; Ishida, M.; Nakajima, T.; Honda, Y.; Kitao, O.; Nakai, H.; Vreven, T.; Montgomery, Jr., J. A.; Peralta, J. E.; Ogliaro, F.; Bearpark, M.; Heyd, J. J.; Brothers, E.; Kudin, K. N.; Staroverov, V. N.; Kobayashi, R.; Normand, J.; Raghavachari, K.; Rendell, A.; Burant, J. C.; Iyengar, S. S.; Tomasi, J.; Cossi, M.; Rega, N.; Millam, J. M.; Klene, M.; Knox, J. E.; Cross, J. B.; Bakken, V.; Adamo, C.; Jaramillo, J.; Gomperts, R.; Stratmann, R. E.; Yazyev, O.; Austin, A. J.; Cammi, R.; Pomelli, C. J.; Ochterski, W.; Martin, R. L.; Morokuma, K.; Zakrzewski, V. G.; Voth, G. A.; Salvador, P.; Dannenberg, J. J.; Dapprich, S.; Daniels, A. D.; Farkas, O.; Foresman, J. B.; Ortiz, J. V.; Cioslowski, J.; Fox, D. J. *Gaussian 09*, revision A.01; Gaussian, Inc.: Wallingford, CT, 2010.
(33) Takano, Y.; Yomogida, A.; Nikawa, H.; Yamada, M.; Wakahara, T.; Tsuchiya, T.; Ishitsuka, M. O.; Maeda, Y.; Akasaka, T.; Kato, T.; Slanina, Z.; Mizorogi, N.; Nagase, S. *J. Am. Chem. Soc.* **2008**, *130*, 16224−16230.
(34) Chaur, M. N.; Valencia, R.; Rodriguez-Fortea, A.; Poblet, J. M.; Echegoyen, L. *Angew. Chem., Int. Ed.* **2009**, *48*, 1425−1428.